

Introduction & Overview

- ❖ Ancient volcanism (>4.35 Ga) on the Moon confirmed
 - Recently: Kalahari 009 and Miller Range 13317 by SIMS Pb-isotopes [1].
 - Previously: Apollo 14 Aluminous Mare Basalts, then Kal 009
 - A14 AMB: Rb-Sr (e.g. [2]), Kal 009: Lu-Hf [3] & Sm-Nd [4].
- ❖ Here: Extend and expand our report on Kal 009 [4].
 - Kal 009 in the context of "secondary lunar crust"
 - A concept introduced by Head and Wilson [5] and continued recently by Whitten and Head [6,7].
 - Here we mean the "original" secondary crust volcanically produced prior to the currently identified lunar basins.
- ❖ Important because the timeline for secondary crust formation may not follow the usual paradigm.
 - i.e., Formation of LMO then Anorthositic crust then Impact Basins then Mare volcanism into the impact basins.
- ❖ When, where, how could such a crust begin forming?
 - Will borrow heavily from prior work on this topic (e.g. [5]-[8]).

Lunar Mare Basalt Meteorite - Kalahari 009

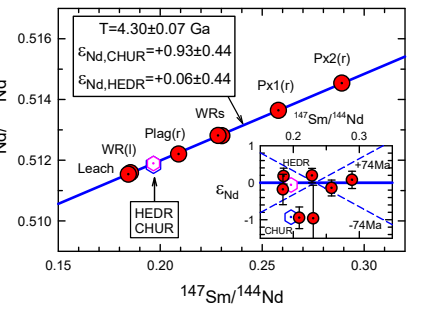


Fig. 1. Sm-Nd age for Kal 009. Data of [4] newly regressed with IsoPlot [11].

Ages of Kalahari 009 Mare Basalt

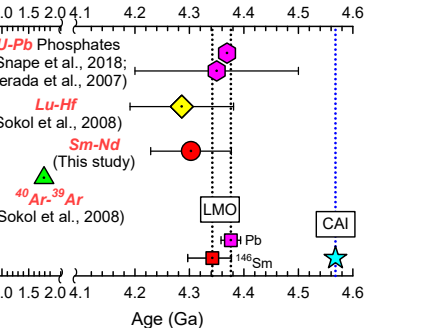


Fig. 2. Upper portion (5 data): Summary of radiometric ages for Kal 009. Lower portion (2 data): Radiometric ages for lunar differentiation ("LMO" age) compared to the solar system age ("CAI" age).

Fig. 5. Estimated lunar global volcanic eruption rate (red) derived from Table 8.9.1 of [16] compared to volcanic production rates [8] after normalizing the estimated maximum production rate to the estimated maximum eruption rate. Horizontal axis shows time in the past (T, Ga) with estimated volcanic extrusion rates (R) from [16] plotted versus the ages of the lunar provinces considered. With terminology from [16]: A = Uplands, B = Procellarum + Tranquillitatis + Fecunditatis + Mendeleev + Schiller, C = Smythii + Humorum + Balmer, D = Serenitatis + Crisium + Humboldtianum + Grimaldi + Schroedinger, E = Imbrium + Orientale. Nectaris is not assigned. The ~4.3 Ga age of Kal 009 is plotted on a linear fit to the extrusion rate estimates omitting Nectaris (star) and would represent some of the oldest secondary volcanic crust in this model.

Lunar Mare Basalt Source Formation

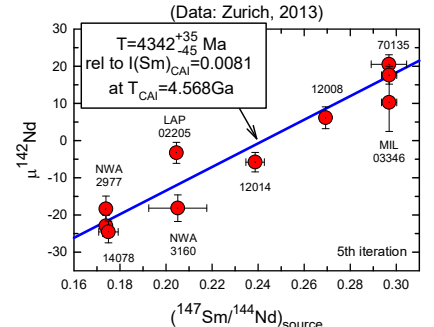


Fig. 3. ¹⁴⁶Sm-¹⁴²Nd isochron for lunar differentiation and formation of mare basalt sources ([14, 15]). Basalts from LREE-enriched sources are at the lower left (¹⁴⁷Sm/¹⁴⁴Nd < CHUR), those from LREE-depleted sources are at the upper right (¹⁴⁷Sm/¹⁴⁴Nd > CHUR).

Kalahari 009, VLT and A14 Aluminous Mare Basalts

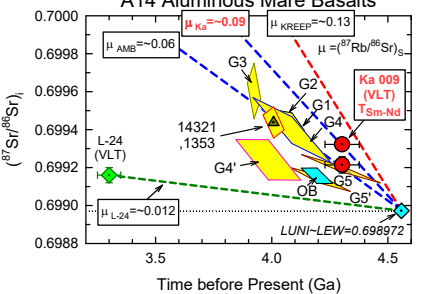


Fig. 4. Conventional (T, t₀) plot for Kal 009, A14 AMB, and Lunar 34 VLT basalts. Comparatively high I_{Sr} values for Kal 009 and A14 AMB suggests derivation from similar, high ⁸⁷Rb/⁸⁶Sr (μ) sources.

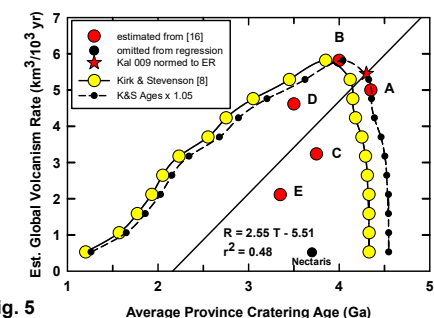


Fig. 5. Estimated lunar global volcanic eruption rate (red) derived from Table 8.9.1 of [16] compared to volcanic production rates [8] after normalizing the estimated maximum production rate to the estimated maximum eruption rate. Horizontal axis shows time in the past (T, Ga) with estimated volcanic extrusion rates (R) from [16] plotted versus the ages of the lunar provinces considered. With terminology from [16]: A = Uplands, B = Procellarum + Tranquillitatis + Fecunditatis + Mendeleev + Schiller, C = Smythii + Humorum + Balmer, D = Serenitatis + Crisium + Humboldtianum + Grimaldi + Schroedinger, E = Imbrium + Orientale. Nectaris is not assigned. The ~4.3 Ga age of Kal 009 is plotted on a linear fit to the extrusion rate estimates omitting Nectaris (star) and would represent some of the oldest secondary volcanic crust in this model.

Mare and SPA units

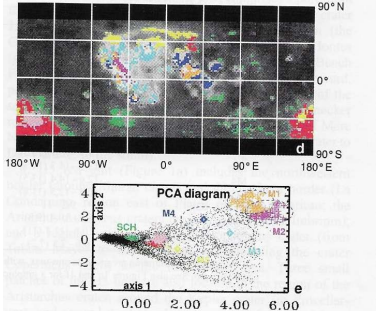


Fig. 6. Lunar global composition from Chevrel et al. [17].

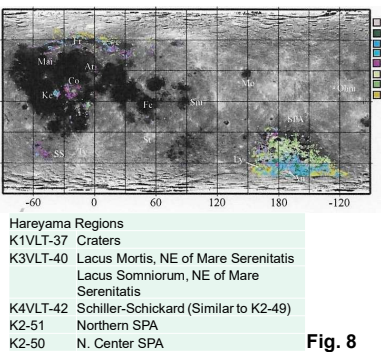


Fig. 7. Principle Component Analysis (XLSTAT®) for remotely-sensed Fe, Ti, and Th abundances. Fig. 8. Lunar global FeO, TiO₂ and Th abundances determined by Hareyama et al. [18] via remote sensing. Fig. 9. PCA applied to the data of Hareyama et al. [18]. Compared to the remote-sensing data, Kal 009 and the Apollo 14 Aluminous Mare basalts have "intermediate" compositions between the lunar crust and mare basalts with high abundances of both Fe and Ti. Higher TiO₂ abundances in the A14 AMB of ~2 wt. % and reference to remote sensing data [19] lead us to redefine "VLT" with TiO₂ < 3 wt. % when considering origins of ancient mare basalts.

Province	Units	Fe	Ti	Th
Highlands	H1	2.7	0.2	0.9
	H2	4.8	0.2	1.3
	H3	6.5	0.2	3.5
	H4	9.0	0.4	5.8
	H5	10.3	0.9	8.0
Mare	M1	14.9	6.5	2.5
	M2	15.3	6.3	3.7
	M3	14.1	3.5	4.0
	M4	13.5	3.5	2.0
	M5	11.4	0.6	3.3
SPA	S1	9.8	0.3	2.3
	S2	11.0	0.55	2.0
	SS	7.2	0.25	1.3

K-mns	TiO ₂	ISODATA
K1	VHT, HT, IMT	N=21
K2	LT, VLT	N=8
K3	VHT, HT, IMT	N=14
K4	VHT, HT, IMT	N=9
K5	Highlands	N=8
K6	Highlands	N=2
K7	Highlands	N=3
S 9	UVHT	00
S = 9	S = 19	S = 66

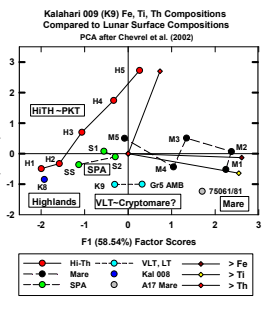


Fig. 8. Lunar global FeO, TiO₂ and Th abundances determined by Hareyama et al. [18]. Compared to the remote-sensing data, Kal 009 and the Apollo 14 Aluminous Mare basalts have "intermediate" compositions between the lunar crust and mare basalts with high abundances of both Fe and Ti. Higher TiO₂ abundances in the A14 AMB of ~2 wt. % and reference to remote sensing data [19] lead us to redefine "VLT" with TiO₂ < 3 wt. % when considering origins of ancient mare basalts.

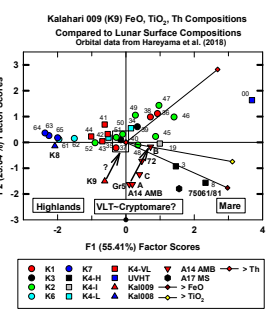


Fig. 9. PCA applied to the data of Hareyama et al. [18]. Compared to the remote-sensing data, Kal 009 and the Apollo 14 Aluminous Mare basalts have "intermediate" compositions between the lunar crust and mare basalts with high abundances of both Fe and Ti. Higher TiO₂ abundances in the A14 AMB of ~2 wt. % and reference to remote sensing data [19] lead us to redefine "VLT" with TiO₂ < 3 wt. % when considering origins of ancient mare basalts.

Table 1. Candidate sources of Kal 009 & MIL 13317

Name	Lat. N ^a	Long. E ^a	Area ^a	Vol. ^b	Age (Ga)
Balmer	-18.74	68.78	6.11	18.3	~3.84
L-F ^d	19.3	106.9	11.3	22.6	~4.01
Smythii	-1.94	85.12	3.88	15.5	~3.90
W.	-21.52	-56.87	0.32	0.16	
Hum.					
SS ^e	-48.8	-51.75	13.2	39.7	~3.77
Kal 009					~4.30 ^c
	^a (10 ⁴ km ²)	^b (10 ⁴ km ³)	^c Sm-Nd isochron		
			^d Lomonosov-Fleming		^e Schiller-Schickard

References: [1] Snape J. F. et al. (2018) *EPSL*, 502, 84-95. [2] Taylor L. A. (1983) *EPSL*, 66, 33-47. [3] Sokol A. K. et al. (2008) *GCA*, 72, 4845-4873. [4] Shih C.-Y. et al. (2008) *LPS XXXIX*, abstract #2165. [5] Head J. W. and Wilson L. (1992) *GCA*, 56, 2155-2175. [6] Whitten J. L. and Head J. W. (2015) *Planet. Space Sci.*, 106, 67-81. [7] Kirk R. L. and Stevenson D. J. (1989) *JGR*, 95, 12,133-12,144. [8] Jacobsen S.B. and Wasserburg G.J. (1984) *EPSL*, 67, 137-150. [9] Nyquist L. E. et al. (2010) *GLUC*, 2010.1.1.A.4. [10] Lugwig K. R. (2008) *Isoplot/EX ver. 3.70*, Berkeley B. G. Center. [11] Borg L. E. et al. (2015) *Meteoritics & Planet. Sci.*, 50, 715-732. [12] Borg L. E. et al. (2016) *EPSL*, 451, 140-158. [13] Nyquist L. E. et al. (1995) *GCA*, 59, 2817-2837. [14] This study (Touboul M. and Kleine T. (2018) pers. comm.) [15] Hartman W. K. et al. (1981) in *BVSP*, 1049-1127. [16] Chevrel S.D. et al. (2002) *JGR*, 107, No. E12, 15-1 to 15-14. [17] Hareyama et al. (2019) *Icarus* 321, 407-425. [18] Prettyman T.H. et al. (2006) *J. Geophys. Res.*, Vol. 111, No. E12, E12007.